JACS
JOURNAL OF THE AMERICAN CHEMICAL SOCIETY
pubs.acs.org/JACS

Article

Redox Control in a Conducting MOF through Coupled Electronic−Vibronic Effects

Darsi Rambabu, Cristian Morari, Augustin Ramackers, Tom Goossens, Vasudeva Rao Bakuru, Petru Apostol, Robert Markowski, Xiaolong Guo, Nagaraju Nakka, Da Tie, Xiaodong Lin, Viliam Frano, Andrii Kachmar, Shubhadeep Pal, Mihaela Buga,* and Alexandru Vlad*

Cite This: https://doi.org/10.1021/jacs.5c20277

Read Online

ACCESS | Metrics & More | Article Recommendations | Supporting Information

ABSTRACT: Redox control in electrically conducting metal−organic frameworks (MOFs) requires understanding how intercalated cations reshape both electronic structure and lattice thermodynamics. In the nominal A_2-Mn-DOBDC anionic framework (A = Li^+, Na^+, K^+), redox potentials and electronic conductivities follow K < Li < Na, contradicting an electrostatic polarization model. Finite-temperature free-energy partitioning shows competing contributions: ΔF_{EL} (electronic term) decreases along Li > Na > K, whereas ΔF_{VIB} (vibrational term) increases along Li < Na < K, producing a maximum stabilization that favors Na and rationalizes the nonintuitive potential ordering. FTIR band shifts track cation-induced systematic mode shifts consistent with cation-dependent vibrational reorganization, and DFT vibrational densities of states with Helmholtz free energies reproduce ΔF_{VIB} trends. Mixed-valence charge transfer with cation-modulated electronic coupling accounts for the conductivity ordering. Na_2-Mn-DOBDC delivers a median discharge voltage of ∼3.0 V vs Na^+/Na while retaining measurable electronic conductivity, providing a general electronic−vibronic route to tune redox energetics in conducting MOFs.

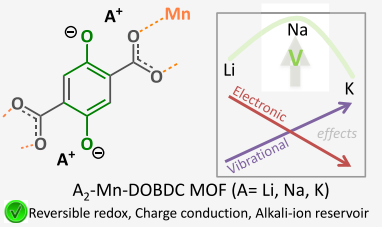

INTRODUCTION

Metal−organic frameworks (MOFs) emerge as versatile positive electrode materials for next-generation electrochemical energy storage.[1−7] Their tunable structure, compositional flexibility, and stability can enable charge storage via both metal centers and organic ligands, leading to competitive energy storage metrics.[8,9] The porous architecture supports ion transport, while the polymeric-like framework enhances cycling stability.[1] Moreover, recent developments have shown that MOFs can be engineered for electronic, ionic, or mixed conductivity, reducing reliance on conductive carbon additives and enabling fast charge−discharge kinetics.[1,3,10−13] For alkali-ion storage, MOFs have been studied as both positive and negative electrodes.[4−7,10,14,15] However, developing cation-reservoir MOF electrodes remains challenging, requiring innovative designs to optimize structure, composition, and electrochemical properties.[1−3]

In spite of many developments, alkali-ion-containing MOF electrode materials remain rare (Scheme 1),[1−3] with redox activity arising from either the anionic organic framework or metal nodes, and alkali cations acting as charge compensators. Only a limited number of MOFs have been reported as cation containing (or cation reservoir) positive electrode materials, underscoring their potential and the need for continued investigation. For example, Li_2-M-DOBDC (M = Mn, Mg),[1] among the first to be developed, was reported to exhibit a one-electron reversible redox, at an average potential of 3.2 V vs Li^+/Li. The Li_2-Mn-DOBDC phase also displayed a measurable 10^{-7} S/cm electrical conductivity at 293 K, 6 orders of magnitude higher than Li_2-Mg-DOBDC, emphasizing the role of redox-active metal ions in controlling the electronic conductivity. Note that Li_2-Mn-DOBDC was found to exhibit structural similarity to Mg(Li_2)-p-DHT,[16,17] whereas Li_2-Mg-DOBDC[1] adopted a distinct polymorph, emphasizing the structure impact on the electrochemical properties. Later, a MIL-53 type MOF was introduced in the form of Li_3-M-O-(DOBDC), [M = Al^{3+}, Fe^{3+}] or MIL-53(M)-$(OLi)_2$,[2] which was found to display a lower redox potential (2.55 V vs Li^+/Li). Finally, a A_4-Zn-DOBDP[3] MOF was suggested recently, supporting a two-electron redox process per ligand, with redox potentials of 3.0 V vs Li^+/Li and ∼2.5 V vs Na^+/Na. This phase was also found to exhibit alkali-ion conductivity (10^{-8} S/cm at 293 K), further advancing MOF-based cathode materials. This progression underscores the growing interest in alkali-ion MOFs as promising electrode materials for energy storage. However, key challenges remain, including improving electronic conductivity, enabling faster alkali-ion transport, and stabilizing high-voltage redox processes. Additionally, exploring the electrode potential by varying A^+ cations within the same

Received: November 14, 2025
Revised: April 22, 2026
Accepted: April 30, 2026

Scheme 1. Evolution of Alkali-Ion Containing MOFs as Positive Electrode Materials and Their Main Performance Metrics[a]

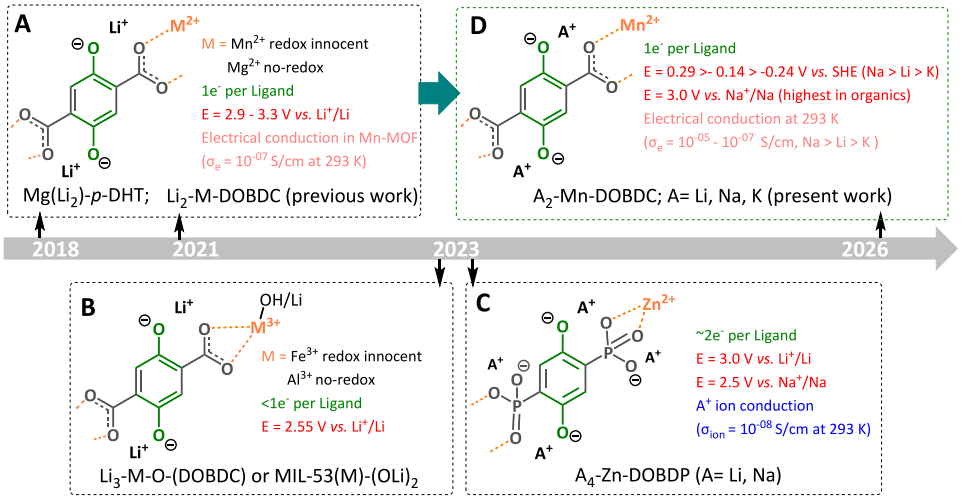

[a](A) Li_2-M-DOBDC,[1,16,17] (B) Li_3-M-O-(DOBDC) or MIL-53(M)-$(OLi)_2$,[2] (C) A_4-Zn-DOBDP,[3] (D) presented in this work, A_2-M-DOBDC. "E" denotes the median discharge voltage.

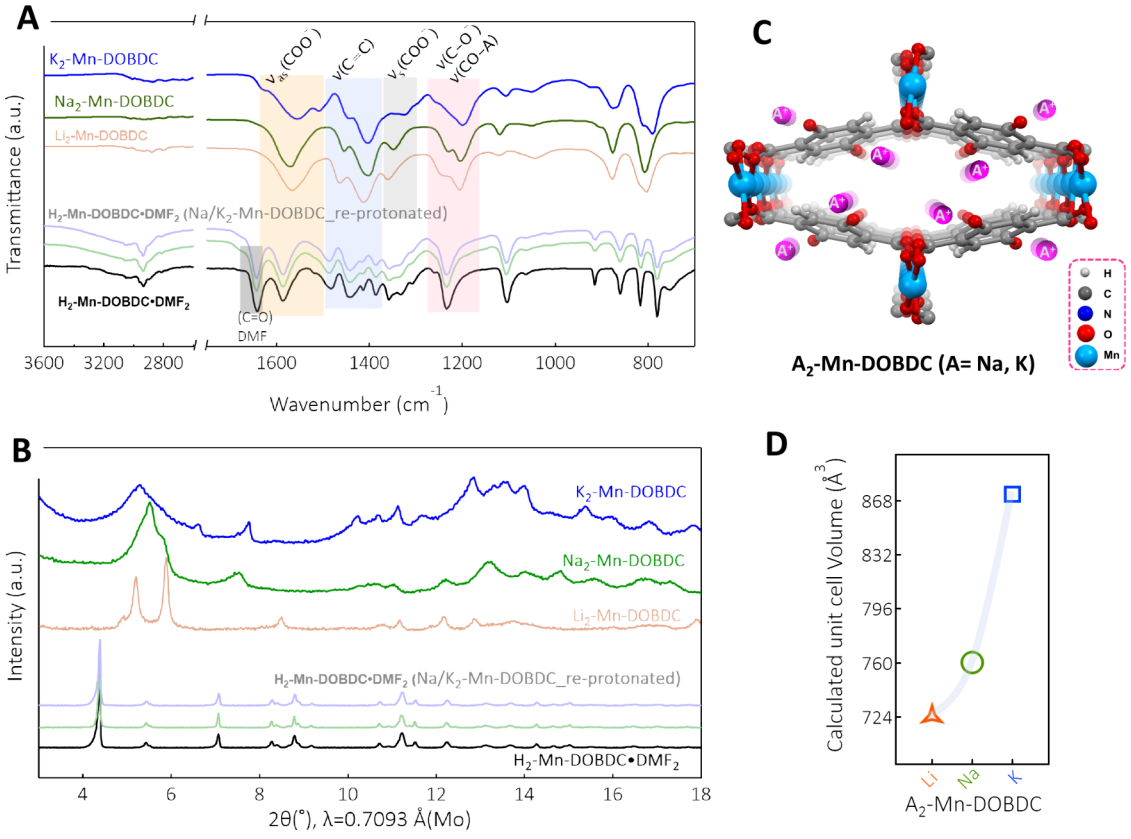

Figure 1. (A) Overlaid FTIR spectra and (B) PXRD patterns of H_2-Mn-DOBDC·DMF_2, A_2-Mn-DOBDC, and reprotonated A_2-Mn-DOBDC phases, demonstrating successful synthesis and reversibility of alkali-proton exchange. Data for the Li_2-Mn-DOBDC[1] phase are included for comparison. (C) Simulated structure of A_2-Mn-DOBDC and (D) DFT-optimized unit cell volume comparisons for A_2-Mn-DOBDC phases studied in this work.

anionic framework can provide fundamental insights into identifying better candidates for alkali-ion-containing MOFs capable of high-voltage operation.

Here, we expanded the investigation of Li_2-Mn-DOBDC by designing Na- and K-ion containing phases, forming A_2-Mn-DOBDC ($DOBDC^{4-}$ = 2,5-dioxido-1,4-benzenedicarboxylate; A = Li^+, Na^+, K^+). Synthesis proceeds with successful incorporation of all studied cations, as supported by elemental analysis and ICP-OES, with compositions close to the nominal A_2 stoichiometry and minimal alkali deficiency ($x \approx 1.6-1.9$; Table S1). Structurally, however, several changes are observed. When compared to pristine protonated H_2-Mn-DOBDC MOF, distinct structural changes occur upon cation exchange, with however the initial phase being recovered upon

https://doi.org/10.1021/jacs.5c20277
J. Am. Chem. Soc. XXXX, XXX, XXX−XXX

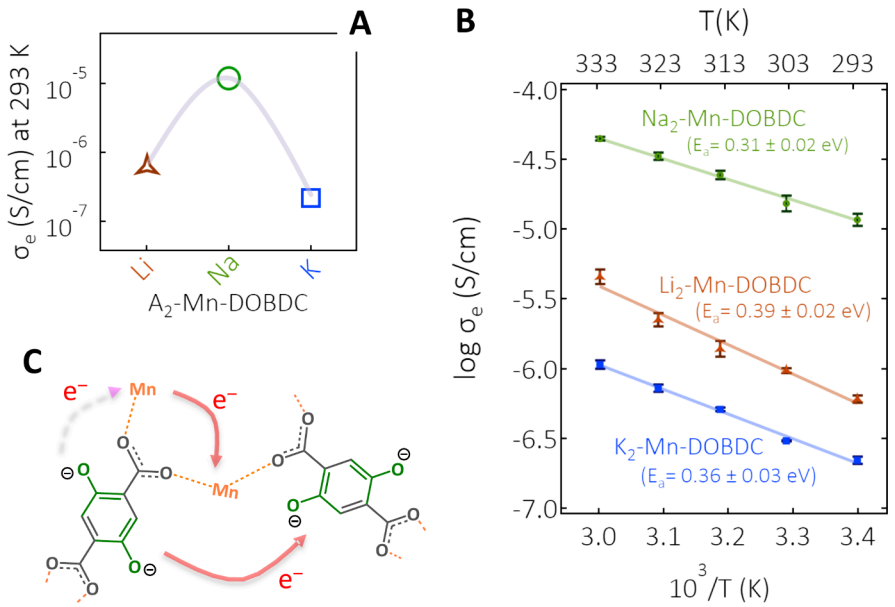

Figure 2. Charge conduction in A_2-Mn-DOBDC (A = Li^+, Na^+, K^+). (A) Room-temperature (293 K) electronic conductivity of A_2-Mn-DOBDC phases. (B) Variable-temperature electronic conductivity plots for A_2-Mn-DOBDC, with activation energies (E_a). Data for the Li_2-Mn-DOBDC phase are included for comparison.[1] (C) Proposed schematic for the mixed valence electronic transport pathways, where solid arrows indicate hopping/self-exchange between equivalent redox-active sites and dotted arrow indicate ligand−metal charge transfer.

reprotonation for all phases, indicating reversible structure breathing. Interestingly, the redox potentials deviate from the expected trend based on a cation polarization power model (Li > Na > K), instead following Na > Li > K (0.54 > 0.17 > 0.12 V vs SHE), with a similar effect noted on the measured electrical conductivity (Na > Li > K, $1.2 \times 10^{-5} > 6.1 \times 10^{-7} > 2.2 \times 10^{-7}$ S/cm at 293 K). This is found to be the result of combined vibrational (Li < Na < K) and electronic (Li > Na > K) effects on the lattice, as revealed by FTIR and DFT analyses.[18] As a Na-reservoir electrode material for sodium batteries, the Na_2-Mn-DOBDC phase exhibits a high median discharge voltage of 3.0 V vs Na^+/Na, surpassing all previously reported Na-ion-containing organic, metal−organic compounds, or MOF phases for Na-ion storage. At a rate of 0.1C, the Na_2-Mn-DOBDC electrode delivers an initial capacity of 89 mAh/g, corresponding to 0.98 e^-, close to the theoretical one-electron capacity of 91 mAh/g, and retains 58% of this capacity after 500 cycles.

RESULTS AND DISCUSSION

Synthesis and Physicochemical Analysis of A_2-Mn-DOBDC MOFs

For the synthesis of A_2-Mn-DOBDC (A = Na^+, K^+) phases we adopted a stepwise postsynthetic MOF modification approach with slight, cation dependent modification procedures, based on our previous protocol (refer to Supporting Information for experimental details).[1] The first step was the synthesis of H_2-Mn-DOBDC·DMF_2, wherein the Mn(II) nodes are coordinated octahedrally with four H_2-$DOBDC^{2-}$ linkers in the equatorial position and two DMF molecules at axial position. The carboxylate groups of H_2-$DOBDC^{2-}$ act as bidentate linkers bridging two Mn(II) nodes, with the uncoordinated pendant phenolic −OH groups of H_2-$DOBDC^{2-}$ pointing inside the square-shaped channels (Scheme S1). After desolvation, the quantitative deprotonation and alkali exchange was confirmed by the complete disappearance of the broad phenolic-OH band along with the ν_{C-OH} deformation bands located at ∼3200 cm^{-1} and 1230 cm^{-1} (Figure 1A). The appearance of the $\nu_{C\text{-}OA}$ vibration bands at 1204 and 1200 cm^{-1} for Na_2- and K_2-phases respectively, indicates formation of phenolate-OA groups. The congruence of A_2-Mn-DOBDC FTIR spectra indicates that the framework remains robust after alkali exchange, while the small shift of the carboxylate, aromatic and phenolate bands are clearly cation-induced, reflecting the influence of the exchanged alkali metal on the local bonding environment, dependent on the nature of cation (vide infra in electrochemical discussion section). Elemental (C, H) and ICP-OES analyses revealed that the compositions are close to the expected values, with Mn:A ratio in the range of 1:1.9−1.6 (Li to K) for A_2-Mn-DOBDC, supporting nominal A_2- framework with systematic alkali deficiency/vacancies ($x < 2$, see Table S1 and accompanying description for details).

Structural analysis revealed a noticeable shift of the low angle peak from 4.4° (in H_2-Mn-DOBDC·DMF_2) to 5.5° and 5.3° in Na_2/K_2-Mn-DOBDC (5.2° 2θ for comparison, in Li_2-Mn-DOBDC) implying a structural distortion during the alkali-proton exchange, resulting in a compact framework (Figure 1B). Compared to pristine H_2-Mn-DOBDC·DMF_2 framework, the Li_2-, Na_2-, and K_2-phases undergo different structural changes upon alkali cation exchange (Figure 1B), due to different coordination environment and size of alkali cations. The DFT-optimized structure analysis indeed shows a progressively increasing unit cell volume for the alkali cation series, consistent with the cation radius ($Li^+ < Na^+ < K^+$, Figure 1D, Table S7). The optimized structures (refer to the DFT section in the Supporting Information for details) also displayed lattice distortion, resulting in a more compact structure compared to the pristine framework (Figure 1C, Scheme S1). Despite these changes, all A_2-Mn-DOBDC phases demonstrate chemical and structural reversibility upon cation-proton exchange, as reprotonation with para-toluene sulfonic acid in DMF restores the initial H_2-Mn-DOBDC·DMF_2 phase,

https://doi.org/10.1021/jacs.5c20277
J. Am. Chem. Soc. XXXX, XXX, XXX−XXX

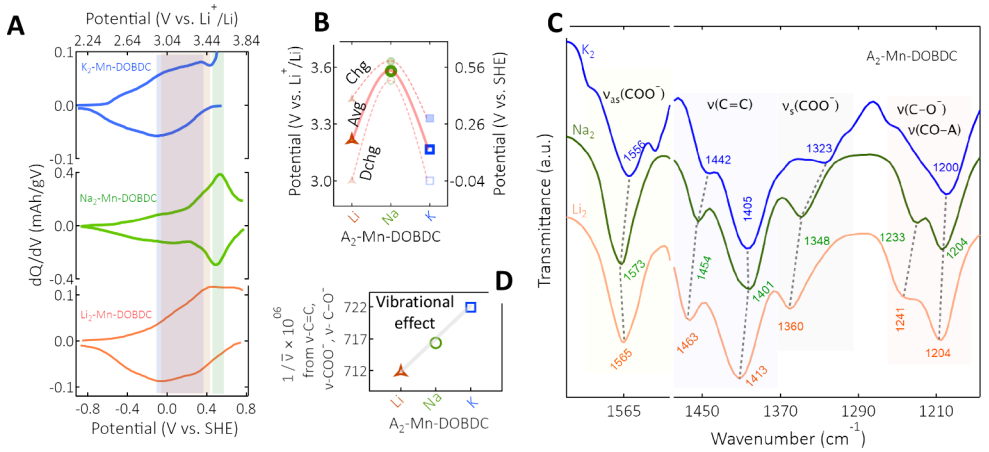

Figure 3. Electrochemical and vibrational analysis of A_2-Mn-DOBDC phases: (A) dQ/dV plots of A_2-Mn-DOBDC electrodes referenced vs Li^+/Li and the standard hydrogen electrode (SHE) for direct comparison. (B) Estimated average charge and discharge electrode potentials. (C) FTIR spectra highlighting the influence (red shift Li to K) of cation type on vibrational modes, including ν(C═C), ν_s(COO^-), and ν(C−O^-) bands. (D) Corresponding evaluation of the inverse arithmetic mean ($1/\bar{\nu}$) of wavenumbers (ν, cm^{-1} from (D); ν −C═C, $\nu_{as,s}$ −COO^-, ν −C−O^-) in A_2-Mn-DOBDC.

consistent with the reversible breathing behavior already noted in Li_2-Mn-DOBDC[1] (Figure 1A). These are confirmed by the appearance/disappearance of characteristic vibration bands in FTIR (e.g., $\nu_{C=O}$ for DMF and ν_{C-OH} for phenol) as well as the similarity between PXRD pattern of pristine and reprotonated MOFs (Figure 1B,C). Considering the evidence provided, it is reasonable to deduce that Mn(II) metal nodes are solely coordinated through carboxylates, rather than phenolate groups, and exhibit structural dynamic behavior during the proton ↔ alkali exchange process (Figure 1A,B, Scheme S1).

Electrical Conductivity Analysis of A_2-Mn-DOBDC

Electrical conductivity is essential for electrode materials, as it can reduce the need for conductive carbon in the electrode composition, maximize active material content and contribute to higher energy density. Previous study focused on the influence of secondary building units (SBUs) and cation exchange on charge transport properties in Li_2-M-DOBDC (M = Mg, Mn), where Li_2-Mn-DOBDC exhibited higher conductivity, attributed to the synergy between the redox-active linker and the metal center, promoting electronic conductivity.[1] This study extends the comparison to Na- and K-containing analogues (refer to Supporting Information for experimental details). Among, Na_2-Mn-DOBDC demonstrated the highest room temperature conductivity of (1.1 ± 0.1) × 10^{-5} S/cm, which is 2 orders of magnitude higher than that of Li_2-Mn-DOBDC ((6.2 ± 0.3) × 10^{-7} S/cm) as well as of K_2-Mn-DOBDC ((2.1 ± 0.1) × 10^{-7} S/cm) analogues (Figure 2A). These values are 10^6−10^8 times higher than those of H_2-Mn-DOBDC, Li_2-Mg-DOBDC, and Mn_2-DOBDC (Mn-CPO-27, 10^{-13} S/cm).[1,19] The conductivity trend is found to follow K^+ < Li^+ < Na^+, a behavior that we attribute to cation-type driven framework distortions/defect landscapes that modulate electronic coupling and orbital overlap, i.e., alkali-ion-induced changes in framework topology/coordination environment that ultimately govern charge transport. The DFT analysis (Figure S14 and associated text) predict a similar tendency, indicating closely related band gaps with minor variations depending on the nature of A^+ ions, suggesting a similar charge carrier pathway. Further, to assess possible ionic conduction from alkali ions, potentiostatic electrochemical impedance spectroscopy (PEIS) was used to measure AC conductivity and compared with two-probe DC (I−V) measurements. Both methods yield essentially identical conductivities (Figure S2, Table S3, and associated text), indicating negligible ionic contribution. Thus, the conductivity trend (K^+ < Li^+ < Na^+) is dominated by electronic transport.

Variable-temperature conductivity measurements were also conducted (Figure S1, Figure 2B, Table S4), all displaying a thermally activate transport behavior, with the activation energy of 0.39 ± 0.02 eV for Li_2-, 0.31 ± 0.02 eV for Na_2-, and 0.36 ± 0.03 eV for K_2-analogues (Figure 2B). The presence of donor and acceptor components in A_2-Mn-DOBDC promotes charge-transfer interactions, with additional redox matching and mixed valence contributing to the high electronic conductivity observed. This behavior likely arises from two distinct yet complementary mixed-valence charge transfer pathways,[20] either between the redox-active linker and the redox-active Mn center or via hopping between equivalent redox centers (metal to metal, M−M; ligand to ligand, L−L) (Figure 2C, Figure S3B). Given the close alignment of the ligand-centered and Mn^{2+}/Mn^{3+} redox potentials in this family,[1] ligand ↔ Mn charge transfer can plausibly act as a redox mediation step that generates and maintains mixed-valence configurations. Redox hopping between equivalent redox centers sites is also possible. This mechanism is further supported by the observation that conductivity is maximized at the half-redox state ($E_{1/2}$),[21] with an incremental increase after a ∼0.5 e^- partial oxidation (Figure S3A), consistent with the A_2-Mn-DOBDC one-electron redox limit (vide infra).[1] This also highlights the limited influence of stoichiometry, as A_2-Mn-DOBDC MOFs show slightly lower alkali-ion content from Li to K (1.9 to 1.6), yet higher conductivity at the $E_{1/2}$ state (partially oxidized, ∼0.5 alkali ion per formula unit) indicating that charge transport is primarily governed by the framework redox state rather than the exact alkali-cation stoichiometry (Table S1 and associated discussion).

The projected density of states (PDOS) for A_2-Mn-DOBDC and A_1-Mn-DOBDC (Figure S15A−C) partially supports the hopping transport model. The DOS remains relatively narrow (0.2−0.4 eV) and is mainly localized on redox active phenolate oxygen atoms, carboxylate groups and Mn centers, depending on the number of alkali atoms in the unit cell (Figure S15A−

https://doi.org/10.1021/jacs.5c20277
J. Am. Chem. Soc. XXXX, XXX, XXX−XXX

C). For A_1-Mn-DOBDC, the PDOS shows significant contribution from phenolate oxygen near the Fermi level, along with a small band gap, indicating semiconducting behavior. In contrast, for A_2-Mn-DOBDC, the phenolate oxygen contribution near the Fermi level is depleted. The system exhibits a weak metallic character, meaning the band gap at the Fermi level is very small or nearly closed (depleted but not fully zero). For intermediate compositions (A_x-Mn-DOBDC, where $1 < x < 2$), partial filling of electronic states reduces the band gap and facilitates electron hopping between Mn-centered sites, which supports a hopping-type charge transport mechanism. Redox-hopping can be impeded either by the redox inactivity of Mg in Li_2-Mg-DOBDC or by the redox innocence of phenolate groups when coordinating the transition metal node, as in Mn-CPO-27 (Mn_2-DOBDC) or protonated H_2-Mn-DOBDC (Figure S3B).[1,19] While remaining in the lower conductivity range (10^{-5}–10^{-7} S/cm, A_2-Mn-DOBDC), these results are promising for alkali-ion-containing organic electrode materials, where electronic conductivities typically range from $\sigma = 10^{-10}$ to 10^{-15} S/cm,[22,23] while alkali-ion-containing coordination polymers exhibit conductivities around 10^{-6} to 10^{-7} S/cm (e.g., A_2-Co-PTtSA).[24]

Electrochemical Response of A_2-Mn-DOBDC: Electronic and Vibronic Effects Governing the Redox Potential

The electrochemical behavior of A_2-Mn-DOBDC (A = Li^+, Na^+, K^+) electrodes was next investigated (Figure 3). The potential–composition profiles (galvanostatic charge–discharge, GCD) for each system were measured with the respective A-metal as counter electrode (half-cell configuration) and the data referred to both Li^+/Li and the standard hydrogen electrode (SHE) for direct comparison. The GCD profiles show a polarization trend in the order K > Li > Na (Figure S5A). The dQ/dV analysis of GCD curves (Figure 3A, Figure S5B) reveals ∼100 mV variation, with the order K < Li < Na. While the Li-MOF shows an average potential of 3.215 V versus Li^+/Li, corresponding to 0.175 V versus SHE, an increase is observed when transitioning from to Na-phase, which delivers an average potential of ∼3.25 V versus Na^+/Na (averaged anodic ∼3.3 V and cathodic ∼3.2 V peak voltages vs Na^+/Na upon charging and discharging), equivalent to 3.58 V versus Li^+/Li (0.54 V versus SHE; a 365 mV increase). In contrast, the K-MOF shows no such potential gain, maintaining an average potential of 3.165 V versus Li^+/Li, corresponding to 0.125 V versus SHE, slightly lower than the Li-MOF (Figure 3B). The average redox potential is thus found to follow the trend of K < Li < Na (3.165 < 3.215 < 3.58 vs Li; 0.125 < 0.175 < 0.54 vs SHE) (Figure 3B) that deviates from polarizing power order of studied alkali cations Li > Na > K, expected to have an impact.

To further understand this behavior, the vibrational effects were analyzed using the FTIR data analysis (Figure 3C, Table S2). The asymmetric carboxylate (COO^-) stretching mode shifts in the order Na > Li > K, indicating changes in metal–ligand interactions. In K_2-Mn-DOBDC, two additional shoulder peaks are present at 1620 cm^{-1} and 1508 cm^{-1}, suggesting additional structural distortion and phase-dependent coordination changes. The symmetric COO^- stretching band around 1350 cm^{-1} follows the trend K > Na > Li, suggesting stronger electron withdrawal effects in K_2-Mn-DOBDC. A slight blue shift in aromatic C=C stretching modes indicates increased electron deficiency in Na_2/K_2-Mn-DOBDC compared to Li_2-Mn-DOBDC. The first C=C stretching band (1450 cm^{-1}) shifts in the order K > Na > Li, while the second (1400 cm^{-1}) follows Na ≈ K > Li, reinforcing the electron-deficient nature of Na_2/K_2-Mn-DOBDC. The C–O stretching mode also shifts to lower wavenumbers from Li to Na/K, further confirming increased electron deficiency on the phenolate group in Na_2/K_2-Mn-DOBDC. The electronic density depletion likely enhances electrostatic interactions, influencing redox behavior and contributes to the observed potential increase in Na_2/K_2-Mn-DOBDC. Overall, the FTIR spectra highlight red shifts in key vibrational bands (ν(C=C), $\nu(COO^-)$, and ν(C–O^-)) from Li to K, reflecting cation-induced structural modifications. This vibrational shift can be quantified by plotting the inverse arithmetic mean of wavenumbers ($1/\bar{\nu}$), providing direct insight into the structural influence of different cations (Figure 3D). The vibrational effect ($1/\bar{\nu}$) increases in the order Li → Na → K, supporting the trend Li < Na < K for cation effects on ligand vibrations, while the observed potential trend follows a different order, K < Li < Na.

DFT analysis was next conducted, offering an additional theoretical perspective on the observed electrochemical trends. The vibrational energy contribution to electrochemical potential was calculated using the Nernst formula. A similar trend as the experimental results was attained (Figures 3D and 4), increasing in the order Li < Na < K (refer to the DFT section in the Supporting Information for details).[18] The electronic free energy, representing the electronic effects, was also investigated, revealing the expected trend for the electrochemical potential, i.e., in agreement with the electronegativity (or the polarizing power) of the alkali metals present in each system: Li > Na > K. The combined vibrational and electronic energy contributions were found to exhibit thus a deviation from typical behavior, ultimately leading to the redox potential trend of K < Li < Na. This unexpected yet consistent pattern aligns well with the experimental results (Figures 3B,D and 4), highlighting the combined influence of these energy factors on the observed electrochemical properties.

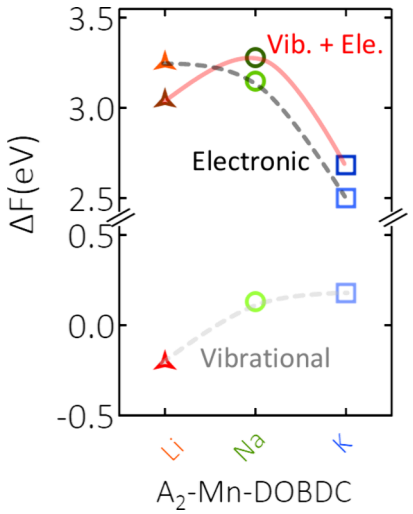

Figure 4. Vibrational and electronic free energies and their combined contribution to the electrochemical potential in A_2-Mn-DOBDC phases.

https://doi.org/10.1021/jacs.5c20277
J. Am. Chem. Soc. XXXX, XXX, XXX–XXX

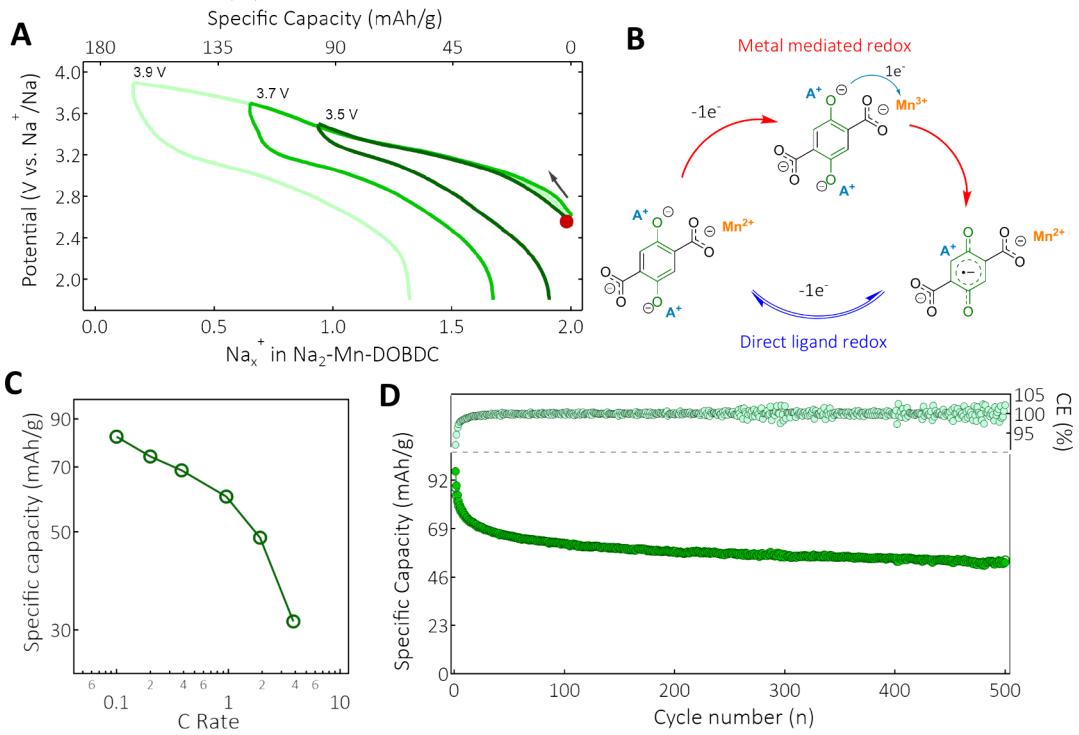

Figure 5. Electrochemical performance and possible redox pathways in Na_2-Mn-DOBDC. (A) Galvanostatic potential−composition profiles of the Na_2-Mn-DOBDC electrode measured in Na-metal half-cell configurations for different potential windows: 1.8−3.5 V, 3.7 V, and 3.9 V vs Na^+/Na. (B) Possible redox pathways in A_2-Mn-DOBDC, distinguishing direct ligand and Mn^{2+}-mediated redox. (C) Ragone-type plot for the capacity retention function of C-rate varied from 0.1C to 4C and (D) capacity retention at 0.1C rate over 500 cycles in Na half-cells (1.8−3.5 V vs Na^+/Na).

Electrochemical Storage Performances of A_2-Mn-DOBDC Positive Electrodes

Considering the possible mixed ligand-Mn redox, the Na^+ storage behavior of Na_2-Mn-DOBDC was first evaluated for three potential windows: 1.8−3.5, 1.8−3.7, and 1.8−3.9 V vs Na^+/Na (Figure 5A). The absence of any discrepancy between DC and AC measurements supports an electron-dominated transport mechanism with negligible long-range ionic contribution (two-probe DC *I*−*V* and PEIS, blocking metallic contacts, no electrochemical driving force); this does not contradict the observed Na^+ ion storage, as ion transport in electrochemical cells occurs primarily through the liquid electrolyte and interfacial processes in an electrolyte-wetted porous electrode, rather than via bulk ionic conduction in a dry pellet (Figure S2, Table S3, and associated text). The voltage profiles display a sloped characteristic, suggesting a solid-solution process,[25−27] consistent with the behavior observed in the Li_2-Mn-DOBDC MOF system.[1] Clear differences in reversibility, electrode polarization, and material utilization are observed for the tested potential ranges, with a reversible exchange of 0.98, 1.02, and 1.16 e^-/Na^+ equivalents achieved for the associated upper cutoff voltages of 3.5, 3.7, and 3.9 V vs Na^+/Na, respectively (Figure 5A). Improved reversibility and stability were particularly observed within the 1.8−3.5 V range (Figure 5A, Figure S6A). This behavior suggests that Na_2-Mn-DOBDC, similar to previously reported Li-based MOF systems,[1,16] is inherently limited to a one-electron redox process, with the extra-capacity extracted originating from either the $Mn^{2+/3+}$ redox couple or the linker's second electron, both being irreversible. The incorporation of Mn^{2+} is also found to significantly raise the redox potential by nearly 900 mV compared to only alkali contained $DOBDC^{4-}$ analogue (Na_4-DOBDC),[28] attributed to the high ionic potential and strong polarizing effect of Mn^{2+}.

The redox mechanism primarily proceeds through either direct ligand-centered oxidation, forming A_1-Mn^{2+}-DOBDC (blue path in Figure 5B), or an Mn-mediated pathway (red path in Figure 5B). Notably, a similar Mn-mediated mechanism has been observed during the chemical oxidation of Mn−CPO-27 (Mn_2-DOBDC).[29] Given the close match between the redox potentials of the ligand and the $Mn^{2+/3+}$ couple, the Mn^{2+} center within the A_2-Mn-DOBDC framework can actively engage in the overall redox process. This Mn-mediated route involves the transient formation of Mn^{3+}-DOBDC (A_1-Mn^{3+}-DOBDC), which promotes ligand oxidation, ultimately yielding a semiquinone-stabilized A_1-Mn^{2+}-DOBDC product (red path in Figure 5B).[1]

Within the optimal potential window of 1.8−3.5 V vs Na^+/Na, a C-rate performance test was conducted revealing good capacity retention at increased C-rates (Figure 5C), corroborating the intrinsic electrical conductivity as well as the high diffusion coefficient (D_{avg}), as determined from galvanostatic intermittent titration technique (GITT, Figure S7). Further electrochemical assessments of Na_2-Mn-DOBDC electrodes demonstrate stable charge storage over extended cycles at 0.1C and 0.5C, exhibiting high reversibility (Figure 5D, Figure S8). At 0.1C, the Na_2-Mn-DOBDC electrode delivers an initial capacity of 89 mAh/g, corresponding to 0.98 e^-, close to the theoretical 1-electron storage. The initial Coulombic efficiency (CE) starts at 92% and gradually increases to approximately 99.5% over subsequent cycles, accompanied by an initial capacity decline within the first 5−10 cycles (Figure S6A,

https://doi.org/10.1021/jacs.5c20277
J. Am. Chem. Soc. XXXX, XXX, XXX−XXX

Figure 5D). This early capacity loss can be attributed to irreversible processes during initial cycling, particularly the formation of a cathode electrolyte interphase (CEI) via oxidative reactions between the electrolyte and the organic phase. While the CEI partially stabilizes the cathode surface, its initial formation and associated structural rearrangements likely account for the early capacity fading, after which stable cycling is achieved with a capacity retention of 58% over 500 cycles (Figure 5D). Importantly, Na-metal-derived interfacial processes, including SEI formation and parasitic reactions that generate soluble species, can further chemically or electrochemically influence the cathode. Correspondingly, in situ PXRD reveals that the framework maintains its main structure during cycling, with reversible modulation of a shoulder near ~5.8° (2θ) during Na^+ extraction and insertion, indicating structural flexibility rather than collapse (Figure S6B). Overall, capacity decay arises from a combination of (i) interfacial processes at both cathode and anode (CEI/SEI growth and polarization), (ii) electrolyte-mediated cross-talk that partially reduces active material accessibility, and (iii) minor structural or electronic changes at the electrode level, rather than Na inventory depletion or wholesale framework collapse. At a higher rate of 0.5C, the shorter charge−discharge times kinetically limit both the extent of interfacial side reactions and the utilization of redox-active sites, resulting in a lower initial capacity (66 mAh g^{-1}, 72% of the theoretical one-electron capacity). Despite, the capacity remains stable, with 88% retention over 100 cycles and a high CE of ~99.5% (Figure S8).

The K-ion storage behavior of K_2-Mn-DOBDC was also evaluated in K-metal half-cells, showing an initial reversible exchange of ~0.8 e^-/K^+ per formula unit at 0.1C, comparable to Na- and Li-based analogues (Figure S9). The Coulombic efficiency reached 85% in the first cycle and improved in subsequent cycles. However, gradual capacity fading was observed, likely due to potassium plating/stripping inefficiency and metal−electrolyte interface instability, contributing to a decline in cycling efficiency and reflecting persistent K-metal challenges.[30]

Sodium-ion containing organic positive electrodes are relatively rare, with only seven chemistries reported to date, including this study. The discharge voltage is considered the most practically relevant parameter for comparison with previously reported organic-based systems, and accordingly, the median discharge voltage is used as a benchmark. For Na_2-Mn-DOBDC, the peak-averaged redox potential is ~3.25 V vs Na^+/Na (averaged anodic ~3.3 V and cathodic ~3.2 V vs Na^+/Na upon charging and discharging, dQ/dv analysis, vide supra), which differs from the median discharge voltage. The median discharge voltage, defined as the voltage at 50% of the delivered discharge capacity, serves as a practical operational metric and is approximately ~3.0 V Na^+/Na under the stated conditions. The difference between the peak-averaged redox potential (~3.25 V) and the median discharge voltage (~3.0 V) reflects the finite hysteresis and polarization inherent to the system. Notably, this work represents the second example within the MOF category (Table S5, Figure 6). Within known materials, Na_2-Mn-DOBDC exhibits a median discharge voltage of ~3.0 V vs Na^+/Na with a moderate capacity, making it relevant for high-voltage sodium-ion batteries. Na_2-Co-PTtSA[24] and Na_4-Zn-DOBDP[3] show lower potentials (~2.8 median discharge V and ~2.5 V, respectively) with varying capacities. The data suggest that transition-metal-based

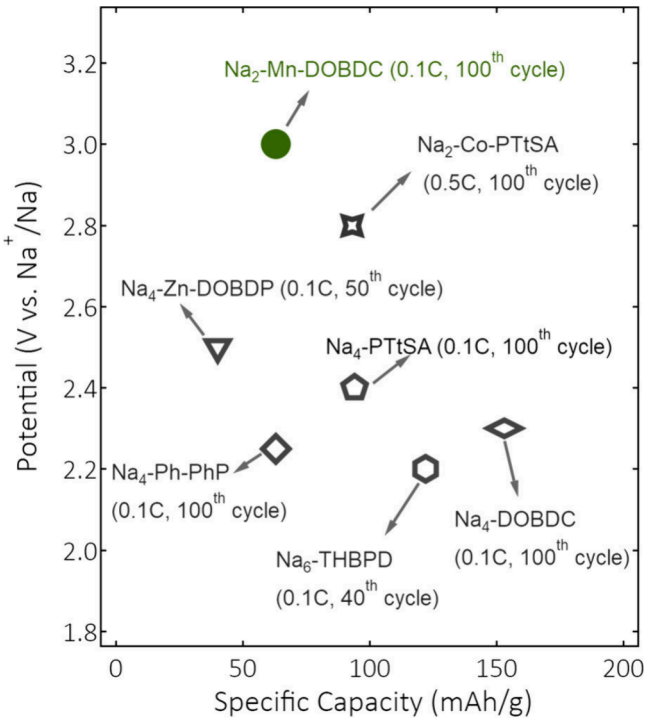

Figure 6. Comparison of median discharge voltage vs capacity performance of Na_2-Mn-DOBDC with sodium-ion-containing MOFs, MOCs (metal−organic compounds), and alkali organic compounds (salts) as positive electrode materials.

frameworks, particularly Zn, Mn, and Co systems, achieve higher working potentials due to spectator cation effects, with Mn and Co also contributing to redox activity and metal−ligand charge transfer. Comparatively, organic-based materials such as Na_6-THBPD,[31] Na_4-Ph-PhP,[32] Na_4-DOBDC,[28] and Na_4-PTtSA[33] exhibit lower potentials (2.2−2.4 V) but retain competitive capacities. These findings highlight the role of structural and electronic modulation in MOFs and MOCs, particularly through transition metal incorporation, in tuning the potential of sodium-ion organic positive electrode materials.

CONCLUSIONS

Cation exchange in A_2-Mn-DOBDC (A^+ = Li^+, Na^+, K^+) MOFs provides a clear demonstration that redox energetics in MOFs cannot be predicted from electrostatic polarization alone. While the conductivity trend (K < Li < Na) can be rationalized by cation-dependent changes in electronic structure, including orbital overlap and electronic coupling within the distorted framework, the redox potential trend (K < Li < Na) emerges from a competition between electronic stabilization and lattice reorganization. This combined electronic−vibronic picture explains why the measured ordering deviates from the expected polarization sequence (Li > Na > K). The mechanistic interpretation is supported experimentally by FTIR band shift analysis and corroborated by DFT, including a temperature-dependent free-energy decomposition that isolates electronic and vibrational contributions to the net potential. Consequently, Na_2-Mn-DOBDC stands out as a promising positive-electrode material, delivering median discharge voltage of 3.0 V vs Na^+/Na (0.29 V vs SHE), outperforming the Li_2- and K_2-analogues. Increasing utilization by accessing the Mn^{2+}/Mn^{3+} node can raise capacity

https://doi.org/10.1021/jacs.5c20277
J. Am. Chem. Soc. XXXX, XXX, XXX−XXX

and voltage but introduces a stability trade-off through faster degradation. Within the optimized operating window, Na-metal cells show stable cycling, retaining 58% of the initial capacity at a rate of 0.1C after 500 cycles. Overall, these results establish cation-programmable structural/electronic tuning, and its coupled vibrational response, as a practical design lever for high-voltage, electronically conducting MOF positive electrodes for energy storage.

■ ASSOCIATED CONTENT

Supporting Information

The Supporting Information is available free of charge at https://pubs.acs.org/doi/10.1021/jacs.5c20277.

Experimental procedures and characterization; electronic conductivity and battery-cycling setups; additional figures and tables; DFT calculation methods and additional discussion (PDF)

■ AUTHOR INFORMATION

Corresponding Authors

Mihaela Buga − *National Research and Development Institute for Cryogenic and Isotopic Technologies—ICSI, ICSI Energy, ROM-EST, 240050 Râmnicu Vâlcea, Romania*; Email: mihaela.buga@icsi.ro

Alexandru Vlad − *Institute of Condensed Matter and Nanosciences, Université Catholique de Louvain, 1348 Louvain-la-Neuve, Belgium; WEL Research Institute, 1300 Wavre, Belgium*; orcid.org/0000-0002-0059-9119; Email: alexandru.vlad@uclouvain.be

Authors

Darsi Rambabu − *Institute of Condensed Matter and Nanosciences, Université Catholique de Louvain, 1348 Louvain-la-Neuve, Belgium*

Cristian Morari − *National Institute for Research and Development of Isotopic and Molecular Technologies, 400293 Cluj-Napoca, Romania*

Augustin Ramackers − *Institute of Condensed Matter and Nanosciences, Université Catholique de Louvain, 1348 Louvain-la-Neuve, Belgium*

Tom Goossens − *Institute of Condensed Matter and Nanosciences, Université Catholique de Louvain, 1348 Louvain-la-Neuve, Belgium*

Vasudeva Rao Bakuru − *Institute of Condensed Matter and Nanosciences, Université Catholique de Louvain, 1348 Louvain-la-Neuve, Belgium*

Petru Apostol − *Institute of Condensed Matter and Nanosciences, Université Catholique de Louvain, 1348 Louvain-la-Neuve, Belgium*; orcid.org/0009-0005-3123-6029

Robert Markowski − *Institute of Condensed Matter and Nanosciences, Université Catholique de Louvain, 1348 Louvain-la-Neuve, Belgium*

Xiaolong Guo − *Institute of Condensed Matter and Nanosciences, Université Catholique de Louvain, 1348 Louvain-la-Neuve, Belgium*

Nagaraju Nakka − *National Research and Development Institute for Cryogenic and Isotopic Technologies—ICSI, ICSI Energy, ROM-EST, 240050 Râmnicu Vâlcea, Romania*

Da Tie − *Institute of Condensed Matter and Nanosciences, Université Catholique de Louvain, 1348 Louvain-la-Neuve, Belgium*

Xiaodong Lin − *Institute of Condensed Matter and Nanosciences, Université Catholique de Louvain, 1348 Louvain-la-Neuve, Belgium*; orcid.org/0000-0002-1867-4789

Viliam Frano − *Institute of Condensed Matter and Nanosciences, Université Catholique de Louvain, 1348 Louvain-la-Neuve, Belgium*

Andrii Kachmar − *Institute of Condensed Matter and Nanosciences, Université Catholique de Louvain, 1348 Louvain-la-Neuve, Belgium*; orcid.org/0000-0002-6819-4820

Shubhadeep Pal − *Institute of Condensed Matter and Nanosciences, Université Catholique de Louvain, 1348 Louvain-la-Neuve, Belgium*; orcid.org/0000-0001-7514-0217

Complete contact information is available at: https://pubs.acs.org/10.1021/jacs.5c20277

Author Contributions

All authors contributed to the conception of the study, data analysis and interpretation, and manuscript preparation, and all authors have approved the final version of the manuscript.

Notes

The authors declare no competing financial interest.

■ ACKNOWLEDGMENTS

This work was supported by F.R.S.-FNRS under the Excellence of Science program (EOS 40007515) and PDR research project (T.0418.26 ORANGE); European Research Council under the European Union's Horizon 2020 research and innovation program (Grant Agreement 770870, MOOiRE); WEL Research Institute (Grant X.9008.25—HECTOR); and R.8001.24 COBRA grant, a M-ERA.NET 3 funding from EU Horizon 2020, GA No. 958174. D.R., V.R.B., and X.L acknowledge F.R.S.-FNRS for Chargé de Recherché (CR) fellowship (Grant Agreements 40010410, 40023657, and 40010559). T.G. and R.M. acknowledges F.R.S.-FNRS for Ph.D. fellowships. D.T. and X.G. acknowledge CSC for the Ph.D. fellowships. C.M. acknowledges the financial support from Project 27N/03.01.2023, Component Project Code PN 23 24 01 04. N.N., M.B., and A.V. acknowledge financial support from the ToNaBatt project, funded by the Romanian Ministry of Research, Innovation and Digitalization within Romania's National Recovery and Resilience Plan (PNRR)—Pillar III, Component C9, Investment I8 (PNRR/2022/C9/MCID/I8), 760113/23.05.2023, and from the Component Project PN 23 15 02 01 (BatNaS) under funding 20N/2023.

■ REFERENCES

(1) Rambabu, D.; Lakraychi, A. E.; Wang, J.; Sieuw, L.; Gupta, D.; Apostol, P.; Chanteux, G.; Goossens, T.; Robeyns, K.; Vlad, A. An Electrically Conducting Li-Ion Metal−Organic Framework. *J. Am. Chem. Soc.* **2021**, *143* (30), 11641−11650.

(2) Denis, M.; Chevreau, H.; Salcedo-Abraira, P.; Moreau, P.; Dupré, N.; Paris, M.; Poizot, P.; Devic, T. Impact of the Metal Centre (Al3+, Fe3+) on the Post-Synthetic Lithiation of Functionalized MIL-53s and the Electrochemical Properties of Lithiated Derivatives. *Mol. Syst. Des. Eng.* **2023**, *8* (8), 1030−1039.

(3) Zhang, Y.; Wang, J.; Apostol, P.; Rambabu, D.; Eddine Lakraychi, A.; Guo, X.; Zhang, X.; Lin, X.; Pal, S.; Rao Bakuru, V.; Chen, X.; Vlad, A. Bimetallic Anionic Organic Frameworks with Solid-State Cation Conduction for Charge Storage Applications. *Angew. Chem., Int. Ed.* **2023**, *62* (42), e202310033.

(4) Zhang, Z.; Awaga, K. Redox-Active Metal-Organic Frameworks as Electrode Materials for Batteries. *MRS Bull.* **2016**, *41* (11), 883−889.
(5) Zhao, R.; Liang, Z.; Zou, R.; Xu, Q. Metal-Organic Frameworks for Batteries. *Joule* **2018**, *2* (11), 2235−2259.
(6) Wang, W.; Chen, D.; Li, F.; Xiao, X.; Xu, Q. Metal-Organic-Framework-Based Materials as Platforms for Energy Applications. *Chem* **2024**, *10* (1), 86−133.
(7) Shrivastav, V.; Sundriyal, S.; Goel, P.; Kaur, H.; Tuteja, S. K.; Vikrant, K.; Kim, K. H.; Tiwari, U. K.; Deep, A. Metal-Organic Frameworks (MOFs) and Their Composites as Electrodes for Lithium Battery Applications: Novel Means for Alternative Energy Storage. *Coord. Chem. Rev.* **2019**, *393*, 48−78.
(8) Zhang, Z.; Yoshikawa, H.; Awaga, K. Monitoring the Solid-State Electrochemistry of Cu(2,7-AQDC) (AQDC = Anthraquinone Dicarboxylate) in a Lithium Battery: Coexistence of Metal and Ligand Redox Activities in a Metal−Organic Framework. *J. Am. Chem. Soc.* **2014**, *136* (46), 16112−16115.
(9) Ziebel, M. E.; Gaggioli, C. A.; Turkiewicz, A. B.; Ryu, W.; Gagliardi, L.; Long, J. R. Effects of Covalency on Anionic Redox Chemistry in Semiquinoid-Based Metal−Organic Frameworks. *J. Am. Chem. Soc.* **2020**, *142* (5), 2653−2664.
(10) Sheberla, D.; Bachman, J. C.; Elias, J. S.; Sun, C. J.; Shao-Horn, Y.; Dincă, M. Conductive MOF Electrodes for Stable Supercapacitors with High Areal Capacitance. *Nat. Mater.* **2017**, *16* (2), 220−224.
(11) D'Alessandro, D. M. Exploiting Redox Activity in Metal-Organic Frameworks: Concepts, Trends and Perspectives. *Chem. Commun.* **2016**, *52* (58), 8957−8971.
(12) Ribeiro, C.; Tan, B.; Figueira, F.; Mendes, R. F.; Calbo, J.; Valente, G.; Escamilla, P.; Paz, F. A. A.; Rocha, J.; Dincă, M.; Souto, M. Mixed Ionic and Electronic Conductivity in a Tetrathiafulvalene-Phosphonate Metal−Organic Framework. *J. Am. Chem. Soc.* **2025**, *147* (1), 63−68.
(13) Rambabu, D.; Goossens, T.; Bakuru, V. R.; Apostol, P.; Mairesse, F.; Steenhaut, T.; Beaujean, P.; Mondal, S. K.; Guo, X.; Zhang, Y.; Pal, S.; Markowski, R.; Lin, X.; Xu, P.; Chanteux, G.; Kachmar, A.; Tie, D.; Ramackers, A.; Frano, V.; Robeyns, K.; Kumar Maji, T.; Filinchuk, Y.; Champagne, B.; Vlad, A. Mixed Proton-Electron Conductivity in a Dynamic 3D Metal-Organic Framework. *Chem* **2025**, *11*, No. 102590.
(14) Wang, Z.; Tao, H.; Yue, Y. Metal-Organic-Framework-Based Cathodes for Enhancing the Electrochemical Performances of Batteries: A Review. *ChemElectroChem* **2019**, *6* (21), 5358−5374.
(15) Wang, D.-Y.; Liu, R.; Guo, W.; Li, G.; Fu, Y. Recent Advances of Organometallic Complexes for Rechargeable Batteries. *Coord. Chem. Rev.* **2021**, *429*, No. 213650.
(16) Jouhara, A.; Dupré, N.; Gaillot, A. C.; Guyomard, D.; Dolhem, F.; Poizot, P. Raising the Redox Potential in Carboxyphenolate-Based Positive Organic Materials via Cation Substitution. *Nat. Commun.* **2018**, *9* (1), 4401.
(17) Shyma Sajeevan, A.; Bernard, L.; Tran-Van, P.; Brandell, D.; Renault, S.; Poizot, P. Combining Polyester-Based Solid Polymer Electrolytes with Lithiated Organic Cathodes for 3.5 V-Class Li-Organic Rechargeable Batteries. *ACS Appl. Polym. Mater.* **2024**, *6* (17), 10102−10112.
(18) Morari, C.; Buimaga-Iarinca, L.; Tripon, C.; Turcu, R. V. F. Comparativestudyofthevibrationalcontributions to Electrochemical Potential in Na2-Mn-DOBDCandLi2-Mn-DOBDCelectrodes. *Electrochim. Acta* **2024**, *473*, No. 143493.
(19) Sun, L.; Hendon, C. H.; Minier, M. A.; Walsh, A.; Dincă, M. Million-Fold Electrical Conductivity Enhancement in Fe 2 (DEBDC) versus Mn 2 (DEBDC) (E = S, O). *J. Am. Chem. Soc.* **2015**, *137* (19), 6164−6167.
(20) Xie, L. S.; Skorupskii, G.; Dincă, M. Electrically Conductive Metal−Organic Frameworks. *Chem. Rev.* **2020**, *120* (16), 8536−8580.
(21) Li, J.; Kumar, A.; Johnson, B. A.; Ott, S. Experimental Manifestation of Redox-Conductivity in Metal-Organic Frameworks and Its Implication for Semiconductor/Insulator Switching. *Nat. Commun.* **2023**, *14* (1), 4388.
(22) Lu, Y.; Chen, J. Prospects of Organic Electrode Materials for Practical Lithium Batteries. *Nat. Rev. Chem.* **2020**, *4*, 127.
(23) Dong, H.; Tutusaus, O.; Liang, Y.; Zhang, Y.; Lebens-Higgins, Z.; Yang, W.; Mohtadi, R.; Yao, Y. High-Power Mg Batteries Enabled by Heterogeneous Enolization Redox Chemistry and Weakly Coordinating Electrolytes. *Nat. Energy* **2020**, *5* (12), 1043−1050.
(24) Wang, J.; Guo, X.; Apostol, P.; Liu, X.; Robeyns, K.; Gence, L.; Morari, C.; Gohy, J.-F.; Vlad, A. High Performance Li-, Na-, and K-Ion Storage in Electrically Conducting Coordination Polymers. *Energy Environ. Sci.* **2022**, *15* (9), 3923−3932.
(25) Steele, B. C. H. In *Superionic Conductors*; Mahan, G. D., Roth, W. L., Ed.; Springer: Heidelberg, 1976; pp 47−64.
(26) Rozier, P.; Morcrette, M.; Martin, P.; Laffont, L.; Tarascon, J.-M. Solid Solution (Li 1.3- y Cu y)V 3 O 8 : Structure and Electrochemistry. *Chem. Mater.* **2005**, *17* (5), 984−991.
(27) Liu, T.; Dai, A.; Lu, J.; Yuan, Y.; Xiao, Y.; Yu, L.; Li, M.; Gim, J.; Ma, L.; Liu, J.; Zhan, C.; Li, L.; Zheng, J.; Ren, Y.; Wu, T.; Shahbazian-Yassar, R.; Wen, J.; Pan, F.; Amine, K. Correlation between Manganese Dissolution and Dynamic Phase Stability in Spinel-Based Lithium-Ion Battery. *Nat. Commun.* **2019**, *10* (1), 4721.
(28) Wang, S.; Wang, L.; Zhu, Z.; Hu, Z.; Zhao, Q.; Chen, J. All Organic Sodium-Ion Batteries with Na 4 C 8 H 2 O 6. *Angew. Chem.* **2014**, *126* (23), 6002−6006.
(29) Cozzolino, A. F.; Brozek, C. K.; Palmer, R. D.; Yano, J.; Li, M.; Dincă, M. Ligand Redox Non-Innocence in the Stoichiometric Oxidation of Mn 2 (2,5-Dioxidoterephthalate) (Mn-MOF-74). *J. Am. Chem. Soc.* **2014**, *136* (9), 3334−3337.
(30) Sun, J.; Du, Y.; Liu, Y.; Yan, D.; Li, X.; Kim, D. H.; Lin, Z.; Zhou, X. Recent Advances in Potassium Metal Batteries: Electrodes, Interfaces and Electrolytes. *Chem. Soc. Rev.* **2025**, *54* (5), 2543−2594.
(31) Bakuru, V. R.; Apostol, P.; Rambabu, D.; Pal, S.; Lin, X.; Markowski, R.; Goossens, T.; Tie, D.; Kachmar, A.; Zhang, Y.; Chanteux, G.; Vlad, A. A Hexaanionic Carboxyphenolate Framework for High Energy Alkali Cation Storage. *Energy Environ. Sci.* **2025**, *18*, 6131.
(32) Zhang, Y.; Apostol, P.; Rambabu, D.; Guo, X.; Liu, X.; Lin, X.; Xie, H.; Chen, X.; Robeyns, K.; Wang, J.; Wang, J.; Vlad, A. Ionically Conducting Li- and Na-Phosphonates as Organic Electrode Materials for Rechargeable Batteries. *Chem. Sci.* **2025**, *16* (4), 1819−1825.
(33) Wang, J.; Liu, X.; Jia, H.; Apostol, P.; Guo, X.; Lucaccioni, F.; Zhang, X.; Zhu, Q.; Morari, C.; Gohy, J.-F.; Vlad, A. A High-Voltage Organic Framework for High-Performance Na- and K-Ion Batteries. *ACS Energy Lett.* **2022**, *7* (2), 668−674.

https://doi.org/10.1021/jacs.5c20277
J. Am. Chem. Soc. XXXX, XXX, XXX−XXX